Origin of the cusp in the transverse momentum distribution for the process of strong-field ionization

I. A. Ivanov*

Center for Relativistic Laser Science, Institute for Basic Science, Gwangju 500-712, Republic of Korea
and Research School of Physics and Engineering, The Australian National University, Canberra, ACT 0200, Australia

(Received 3 November 2015; published 18 December 2015)

We study the origin of the cusp structure in the transverse or lateral electron momentum distribution (TEMD) for the process of tunneling ionization driven by a linearly polarized laser pulse. We show that the appearance of the cusp in the TEMD can be explained as follows. Projection on the set of the Coulomb scattering states leads to the appearance of elementary cusps which have a simple structure as functions of the lateral momentum. This structure is independent of the detailed dynamics of the ionization process and can be described analytically. These elementary cusps can be used to describe the cusp structure in TEMD.

DOI: 10.1103/PhysRevA.92.063417 PACS number(s): 32.80.Rm, 32.80.Fb, 42.50.Hz

I. INTRODUCTION

The seminal paper by Keldysh [1] laid out the distinction between tunneling and multiphoton regimes in the photoionization process. Keldysh's paradigm proved particularly fruitful for the study of tunneling ionization, a photoionization process characterized by small values of the so-called Keldysh parameter $\gamma = \omega\sqrt{2|\varepsilon_0|}/E$ (here ω, E, and $|\varepsilon_0|$ are the frequency, field strength, and ionization potential of the target system expressed in atomic units). Subsequent developments [2–5] elaborated on various aspects of this approach in the tunneling regime, making it an extremely useful and versatile tool for understanding tunneling photoionization. Comprehensive reviews of these developments (to which we will refer below as tunneling theories) can be found in [6,7].

A remarkable feature of the tunneling regime is that one may still use to some extent the classical notions, such as that of the electron trajectory. This fact has been extensively used in modeling tunneling photoionization. In this approach tunneling photoionization is regarded as a process in which an electron first emerges into the continuum as a result of the under-the-barrier tunneling. This part of the problem is described quantum mechanically, producing probabilistic distributions of the electron's characteristics (typically velocities), which can be used as initial conditions for the subsequent classical modeling describing electron motion after the ionization event. Such a procedure has been used with success to produce ionization spectra in good agreement with experiment [8] for complicated systems where truly *ab initio* treatment becomes hopelessly complicated.

These distributions which weight different initial conditions in the electron's phase space are not themselves observed in the experiment. The electron momentum distribution measured at the detector can, however, provide information about the distributions at the moment of the ionization event, which offers an exciting possibility to look at this event experimentally [9,10]. Of course, from the strict quantum-mechanical point of view the notion of the electron escaping the atom at a particular moment of time should be regarded with some caution [11]; nevertheless, this picture of an electron escaping into the continuum proved extremely fruitful.

Tunneling theories predict simple Gaussian-like structures for these initial distributions. If the after-ionization-event motion is treated as guided by only the laser field (ionic core potential is neglected), the momentum distributions at the detector retain this Gaussian character, with a possible shift of the distribution in the momentum space due to the overall momentum the electron acquires from the laser field after the ionization event [6]. Of particular interest, therefore, is the so-called transverse or lateral electron momentum distribution (TEMD), which describes the distribution of the electron momenta measured at the detector in the direction perpendicular to the polarization plane of the driving pulse. In the simple picture in which electron motion is guided by only the laser field, the TEMD is unaffected by the motion subsequent to the ionization event.

This prediction is not always true. While the TEMD measured at the detector is a Gaussian for the driving pulse with close to circular polarization [12], it looks rather different for the case of linear polarization. It has been found [13] that for the case of the linearly polarized laser pulse the transverse electron momentum distribution exhibits a sharp cusplike peak at zero transverse momentum. We studied this transition from the cusplike to the Gaussian-like structure in TEMD numerically using the *ab initio* solution of the time-dependent Schrödinger equation (TDSE) in [14].

Studying the TEMD can provide other useful information. It has been demonstrated, both experimentally and theoretically [15], that the transverse electron momentum distributions in the tunneling and over-the-barrier ionization regimes (OBI) evolve in markedly different ways when the ellipticity parameter describing the polarization state of the driving laser pulse increases. This fact can be used to make a clear distinction between the tunneling and OBI regimes in the experiment.

In the present work we study the origin of the cusp structure in TEMD for the case of the linearly polarized driving laser pulse in detail. In [13] this structure at zero transverse momentum was attributed to low-energy singularity of the Coulomb wave function [13]. We show that, although this interpretation is basically correct, there is more to the story. Projection on the set of the Coulomb scattering states produces the elementary cusps which have a simple structure as functions of the lateral momentum. This structure can be described analytically. These elementary cusps can be used to describe the cusp structure in TEMD.

*Igor.Ivanov@anu.edu.au

II. THEORY AND RESULTS

We will be guided below to a considerable extent by the numerical results provided by the solution of the TDSE for a hydrogen atom. We will therefore briefly describe the procedure. We solve TDSE for a hydrogen atom in the presence of a laser pulse:

$$i\frac{\partial\Psi(\boldsymbol{r})}{\partial t} = [\hat{H}_{\rm atom} + \hat{H}_{\rm int}(t)]\Psi(\boldsymbol{r}). \tag{1}$$

Operator $\hat{H}_{\rm int}(t)$ in Eq. (1) describes the interaction of the atom with the EM field. We use the velocity form for this operator:

$$\hat{H}_{\rm int}(t) = \boldsymbol{A}(t)\cdot\hat{\boldsymbol{p}}\ , \tag{2}$$

with

$$\boldsymbol{A}(t) = -\int_0^t \boldsymbol{E}(\tau)\,d\tau. \tag{3}$$

The laser pulse is linearly polarized along the z direction, which we use as a quantization axis:

$$E_z = E_0 f(t)\cos\omega t. \tag{4}$$

For the base frequency of the pulse we use $\omega = 0.057$ a.u. (corresponding to a wavelength of 790 nm). The function $f(t) = \sin^2(\pi t/T_1)$ in Eq. (4) (here $T_1 = NT$ is total pulse duration, N is an integer, and $T = 2\pi/\omega$ is an optical cycle of the field). We report below results for various pulse durations T_1 and field strengths E_0. TDSE is solved for a time interval $(0,T_1)$. The initial state of the system is a ground state of the hydrogen atom.

To solve the TDSE we employed the procedure described in Refs. [16,17]. The solution of the TDSE is represented as a series in spherical harmonics:

$$\Psi(\boldsymbol{r},t) = \sum_{l=0}^{L_{\rm max}} f_l(r,t)Y_{l0}(\theta). \tag{5}$$

The radial part of the TDSE is discretized on the grid with a step size $\delta r = 0.1$ a.u. in a box of the size $R_{\rm max} = 600$ a.u. We consider relatively short total pulse durations and moderately strong field intensities (not exceeding six optical cycles and 3.5×10^{14} W/cm^2, respectively). We used $L_{\rm max} = 50$ in the calculations reported below. The necessary checks ensuring that for such field parameters the calculation is well converged with respect to $L_{\rm max}$ and $R_{\rm max}$ have been performed.

Substitution of the expansion (5) into the TDSE gives a system of coupled equations for the radial functions $f_l(r,t)$. To solve this system we use the matrix iteration method [18]. Ionization amplitudes $a(\boldsymbol{p})$ are obtained by projecting the solution of the TDSE at the end of the laser pulse on the set of ingoing scattering states $\psi_{\boldsymbol{p}}^{(-)}(\boldsymbol{r})$ of the hydrogen atom:

$$\Psi_{\boldsymbol{p}}^{(-)}(\boldsymbol{r}) = \sum_{l\mu} i^l e^{-i\eta_l(p)} Y_{l\mu}^*(\boldsymbol{p})Y_{l\mu}(\boldsymbol{r})R_{lp}(r). \tag{6}$$

For the linearly polarized laser pulse and the coordinate system we employ, only the terms with $\mu = 0$ actually contribute to the projection, of course. The differential photoionization cross section is computed as $P(\boldsymbol{p}) = |a(\boldsymbol{p})|^2$. We are interested in the transverse or lateral electron momentum distribution, describing the probability of detecting a photoelectron with a given value of the momentum component $p_\perp$ perpendicular to the polarization plane. Because of the symmetry of the problem due to the linear polarization of the driving pulse any plane containing the polarization vector can be chosen as a polarization plane. Choosing the (y,z) plane as the polarization plane, we obtain, for TEMD as a function of the lateral momentum $p_\perp = p_x$,

$$W(p_\perp) = \int P(p_x,p_y,p_z)\,dp_y\,dp_z. \tag{7}$$

TEMDs obtained using this procedure are shown in Fig. 1 for two sets of the driving pulse parameters.

Distributions obtained following the prescription described above and using the Coulomb ingoing scattering states (6) for the projection operation (solid lines in Fig. 1) show the cusplike behavior at $p_\perp = 0$. While the TEMD remains continuous at this point, its derivative suffers discontinuity. It was suggested in [13] that the cusp originates from the singularity of the Coulomb continuum wave function at zero energy. We subsequently found some numerical evidence [14] supporting this statement. What interests us in the present work is elucidating the nature of the cusp and the precise type of discontinuity which the lateral distribution has at $p_\perp = 0$. As we shall see, some analytical results describing the discontinuity can be obtained.

We begin by presenting results of a few numerical experiments. We first make sure that the cusp is indeed due to the projection on the set of Coulomb continuum wave functions. In Fig. 1 we present results obtained if the same solutions of the TDSE at the end of the laser pulse are projected on the set of the plane waves and the ingoing states of the Yukawa potential $V(r) = -e^{-0.1r}/r$ instead of the Coulomb scattering states. The spectra obtained by using the plane-wave basis and scattering state of the Yukawa potential, although agreeing quantitatively rather well with the spectrum obtained by projecting the solution of the TDSE on the Coulomb scattering states, show no cusplike behavior at $p_\perp = 0$. The cusp arises therefore as a result of the projection operation using the Coulomb scattering states, as was surmised in [13]. The question which interests us is the detailed mechanism responsible for the appearance of the cusp.

We note first that the cusp cannot be introduced by the integration procedure when overlaps between the TDSE solution and the Coulomb scattering states are computed. The amplitude functions $f_l(r,T_1)$ in the expansion of the TDSE solution (5) are square-integrable functions with typical spatial extent corresponding to the distance the outgoing electron wave packet can have traveled by the end of the laser pulse. Integration of such functions cannot introduce any low-energy singular behavior. Indeed, we can consider that, to a good approximation, the amplitude functions $f_l(r,T_1)$ have finite support, being nonzero only in the finite region of space (which is what they are in the numerical calculation anyway). Integration of such functions cannot introduce any new singularities which are not already present in the integrand. We must therefore look carefully at the singularities present in the Coulomb scattering state (6).

There are two factors in Eq. (6) we have to examine: the Coulomb scattering phase shifts and the radial Coulomb wave

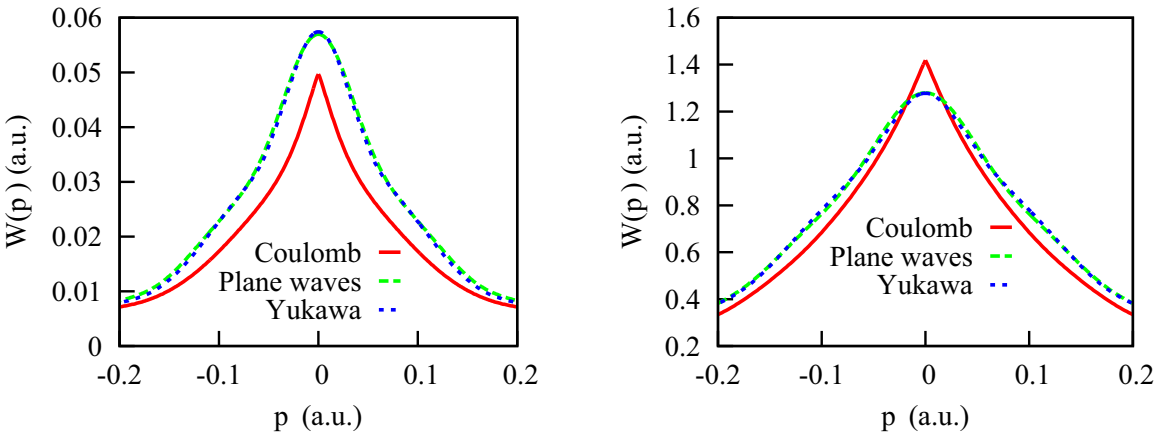

FIG. 1. (Color online) Left: TEMD for the laser pulse (4) with a pulse intensity of 10^{14} W/cm^2 and a total duration of six optical cycles. Right: the same for a field intensity of 3.5×10^{14} W/cm^2 and a pulse duration of four optical cycles. Solid red line: projection on the ingoing Coulomb scattering states (6). Long-dashed green line: projection on the basis of plane waves. Short-dashed blue line: projection on the set of the ingoing scattering states of the Yukawa potential.

functions. The explicit expression for the Coulomb phase shifts reads [19]

$$\eta_l(p) = \arg\Gamma\left(l + 1 - \frac{i}{p}\right), \tag{8}$$

and it exhibits a highly singular behavior at $p = 0$. On the other hand, the radial functions $R_{lp}(r)$ in Eq. (6) can be written [we use the $\delta(\boldsymbol{p} - \boldsymbol{p}')$ normalization] as [19]

$$R_{lp}(r) = \beta(p)\gamma(p)g_{lp}(r), \tag{9}$$

where

$$\gamma(p) = \frac{1}{1 - e^{-\frac{2\pi}{p}}} \tag{10}$$

and

$$\beta(p) = \frac{1}{\sqrt{p}}. \tag{11}$$

The function $g_{lp}(r)$ can be found as the solution of the radial Schrödinger equation satisfying a boundary condition $g_{lp}(r) \to C_l e^{l+1}$ when $r \to 0$ and C_l is a constant factor independent of energy. By the well-known Poincaré theorem $g_{lp}(r)$ is therefore an entire function of energy, i.e., an entire function of p^2. The radial wave function in (6) is singular at $p = 0$ only due to the presence of the factors $\gamma(p)$ and $\beta(p)$ given by Eqs. (10) and (11).

We have thus identified three potential culprits which may introduce singular low-energy behavior and which may be responsible for the formation of a cusp. Let us study them one by one.

Consider first the effect of the Coulomb scattering phase shift. In Fig. 2 we present results of a simple numerical experiment obtained if, in the expression for the Coulomb ingoing scattering state (6), we put $\eta_l(p) = 0$ in the exponential function [and use the correct Coulomb radial wave functions $R_{lp}(r)$].

One can see that removal of the scattering phase shifts $\eta_l(p)$ from Eq. (6) produces hardly any effect on the lateral spectrum. We could, in fact, anticipate this. Indeed, from the expression for the Coulomb phase shifts (8) and elementary properties of the Γ function one can easily deduce the relation $\eta_{l+1}(p) = \eta_l(p) - \frac{\pi}{2} + O(p)$, and hence

$$\eta_{l+1}(p) = \eta_0(p) - \frac{(l+1)\pi}{2} + O(p), \tag{12}$$

which is valid when $p \to 0$. We see thus that at low energies the effect of the Coulomb phase shifts $\eta_l(p)$ in Eq. (6) reduces to introducing an energy-independent phase factor for different terms in the sum in Eq. (6) and overall dependence of the photoionization amplitude on $\eta_0(p)$, which cancels out when we compute the squared modulus of the amplitude. On the other hand, with increasing energy Coulomb phase shifts decrease quickly, which explains the fact that Coulomb phase shifts have virtually no effect on the TEMD. The role of the factor $\gamma(k)$ is equally insignificant, as can be seen from Fig. 2, where we show the spectrum obtained if we put $\gamma(p) = 1$ in Eq. (6). Again, this fact could be anticipated since this factor,

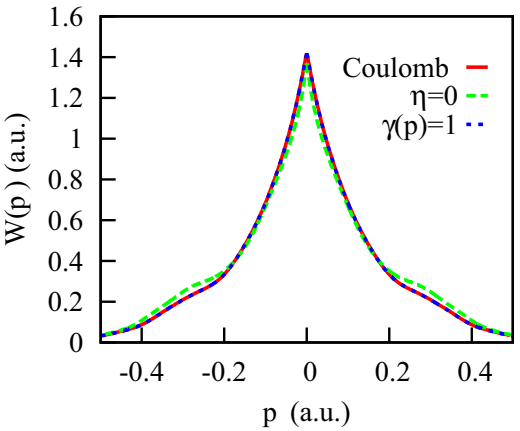

FIG. 2. (Color online) Left: TEMD for the laser pulse (4) with a pulse intensity of 3.5×10^{14} W/cm^2 and a pulse duration of four optical cycles. Solid red line: projection on the correct ingoing Coulomb states (6). Long-dashed green line: projection on the set of states (6) with $\eta_l(p) = 0$. Short-dashed blue line: projection on set of states (6) with $\gamma(p) = 0$.

although singular at $p = 0$, does not blow up at this point and tends to be one with increasing energy.

We are left, therefore, with the only factor in the Eq. (6) which blows up at $p = 0$, the factor $\beta(p)$ in Eq. (11). There are, of course, other factors in Eq. (6) which are singular at $p = 0$. The spherical harmonics $Y_{l\mu}(\boldsymbol{p})$ are, strictly speaking, singular functions of the components of the vector $\boldsymbol{p}$ at $\boldsymbol{p} = 0$ because of the coordinate system singularity at this point. Similarly, the higher-order terms in Eq. (12) are proportional to p, and in a strict mathematical sense the function p is singular at $\boldsymbol{p} = 0$ as a function of the components of the vector $\boldsymbol{p}$. These singularities are, however, only mild ones; in particular they do not lead to the unbounded growth of the function. The only singularity which does lead to such a growth is the one due to the factor $\beta(p)$.

We are now in a position to elucidate the nature of the cusp in the lateral distribution. To this end, let us note that because of the symmetry of the problem the differential photoionization cross section $P(\boldsymbol{p})$ is, in fact, a function of only two variables: $P(\boldsymbol{p}) = P(p, \cos\theta)$, where θ is the angle between electron momentum $\boldsymbol{p}$ and the z axis. Expanding this expression in powers of θ, we may write for the differential cross section

$$P(\boldsymbol{p}) = \sum_{n=0}^{\infty} P_n(p) \cos^n \theta, \tag{13}$$

where $P_n(p)$ are functions of only p. Coefficients of this expansion can be computed numerically from the known solution of the TDSE by reexpanding products of the spherical harmonics $Y_{l\mu}(\boldsymbol{p})$ occurring in the expression for the squared modulus of the amplitude $|a(\boldsymbol{p})|^2$ in series of spherical harmonics with the help of the well-known formulas and reexpanding in turn the resulting spherical harmonics in powers of $\cos\theta$. The important point here is that coefficients $P_n(p)$ depend only on p and inherit from the amplitudes the singular behavior at $p = 0$ due to the factor $\beta(p)$ in Eq. (11). The $p^{-\frac{1}{2}}$ singular behavior of the amplitudes at $\boldsymbol{p} = 0$ clearly entails the p^{-1} singular behavior of the coefficients $P_n(p)$ at $p = 0$. Integrating Eq. (13) over the (p_y, p_z) plane (only terms with even n give nonzero contributions, of course), we obtain for the TEMD

$$W(p_\perp) = \sum_{n=0,2,\ldots}^{\infty} W_n(p_\perp)\,, \tag{14}$$

where

$$\begin{aligned} W_n(p_\perp) &= \int_0^\infty dq \int_0^{2\pi} d\phi q\, P_n(p) \left(\frac{q\cos\phi}{p}\right)^n \\ &= \frac{2\pi n!}{\Gamma(n/2+1)^2 2^{n-1}} \int_0^\infty dq\, P_n(p) \frac{q^{n+1}}{(p_\perp^2+q^2)^{\frac{n}{2}}}, \end{aligned} \tag{15}$$

where $p = \sqrt{p_\perp^2 + q^2}$ and we used a cylindrical coordinate system (q,ϕ) in the (p_y, p_z) plane.

Using Eq. (15), we can obtain asymptotic behavior of $W_n(p_\perp)$ for $p_\perp \to 0$. As we mentioned above, $P_n(p)$ behaves as p^{-1} for small energies. Let us choose some small positive Q and represent $P_n(p)$ in the interval $(0, Q)$ as $P_n(p) = C_n/p + P_n'(p)$, where $P_n'(p)$ is nonsingular at $p = 0$. Singular behavior of the integrals in Eq. (15) at $p_\perp = 0$ can appear only as a result of the integration of the singular term C_n/p in $P_n(p)$ over the interval $(0, Q)$. Indeed, the integrands in both the integral over the interval $(0,\infty)$ with $P_n'(p)$ and the integral over the interval (Q,∞) with C_n/p contain smooth regular functions as integrands, which cannot lead to a small-$p_\perp$ singular behavior. We can write therefore

$$W_n(p_\perp) = C_n I_n(p_\perp, Q) + W_n^{\mathrm{reg}}(p_\perp), \tag{16}$$

where

$$I_n(p_\perp, Q) = \int_0^Q dq \frac{q^{n+1}}{(p_\perp^2+q^2)^{\frac{n+1}{2}}}. \tag{17}$$

C_n is a constant, and $W_n^{\mathrm{reg}}(p_\perp)$ are nonsingular at $p_\perp = 0$, behaving near this point as $W_n^{\mathrm{reg}}(p_\perp) \approx u_n^0 + u_n^2 p_\perp^2$ with some constants u_n^0 and u_n^2.

It is clear from Eq. (17) why this contribution becomes singular at $p_\perp = 0$. While the integral has a finite value if we put $p_\perp = 0$, an attempt to calculate the derivative with respect to $p_\perp$ by differentiating under the integral sign leads to a divergent expression. We have to be more careful in evaluating the asymptotic of the integral. Using well-known formulas for the integral representation and asymptotic properties of the hypergeometric function $F(a,b;c;z)$ [20], we obtain

$$\begin{aligned} I_n(p_\perp, Q) &= \frac{Q^{n+2}}{2|p_\perp|^{n+1}} \frac{\Gamma\left(\frac{n}{2}+1\right)\Gamma\left(\frac{1}{2}\right)}{\Gamma\left(\frac{n}{2}+\frac{3}{2}\right)} \\ &\quad \times F\left(\frac{n+1}{2}, \frac{n}{2}+1; \frac{n}{2}+\frac{3}{2}; -\frac{Q^2}{p_\perp^2}\right) \\ &\approx A_n + B_n|p_\perp| \quad p_\perp \to 0\,, \end{aligned} \tag{18}$$

where we do not give explicit expressions for the unimportant constant factors.

From Eqs. (16) and (18) we conclude that $W_n(p_\perp)$ behave, for small $p_\perp$, as linear functions of $|p_\perp|$:

$$W_n(p_\perp, Q) = g_n + h_n|p_\perp| + O(p_\perp^2) \quad p_\perp \to 0\,, \tag{19}$$

where g_n and h_n are some constants. This implies the following cusp structure of $W_n(p_\perp)$ at $p_\perp = 0$. The first derivative of $W_n(p_\perp)$ with respect to $p_\perp$ is discontinuous at $p_\perp = 0$; the second derivative is therefore infinite. That this formula indeed reproduces asymptotic behavior correctly can be seen from Fig. 3. The contributions $W_n(p_\perp)$ as functions of lateral momentum obtained from the TDSE calculation are shown in Fig. 3. $W_n(p_\perp)$ vary considerably with n in magnitude and need not be positive; to facilitate the comparison we present the scaled contributions: $W_n(p_\perp)/|W_n(0)|$. In Fig. 3 we present also the results of the linear fits: $W_n(p_\perp)/|W_n(0)| = A + B|p_\perp|$.

Two features are apparent from Fig. 3. First, for small values of $p_\perp$ the contributions $W_n(p_\perp)$ are indeed linear functions of $|p_\perp|$, in agreement with the asymptotic estimate (19) we made above. Second, the region where this asymptotic estimate represents $W_n(p_\perp)$ accurately shrinks with n. There is, of course, nothing unusual in such behavior. Asymptotic estimates give us asymptotic behavior for small values of a parameter, but they do not necessarily tell us how small the parameter should be for the estimate to be accurate. A glance at the behavior of the integrals in Eq. (17) as functions of lateral momentum

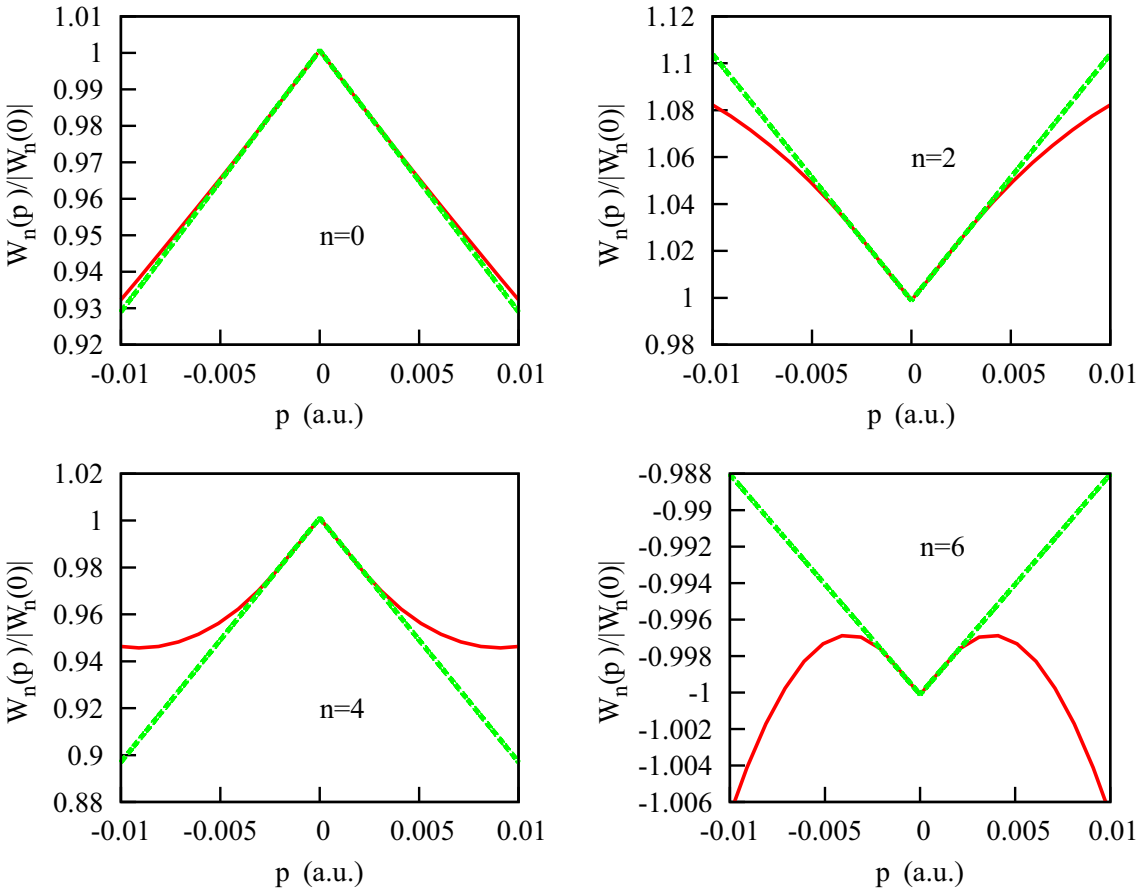

FIG. 3. (Color online) Solid red line: scaled terms of the series (14) $W_n(p_\perp)/|W_n(0)|$ as functions of lateral momentum $p_\perp$. Dashed green line: linear fit, $W_n(p_\perp)/|W_n(0)| = A + B|p_\perp|$. Field intensity is 3.5×10^{14} W/cm^2; pulse duration is four optical cycles.

may help us to understand what is happening. We show in Fig. 4 integrals $I_n(p_\perp, Q)$ as functions of $p_\perp$ for a fixed value of $Q = 0.05$ a.u. Figure 4 shows qualitatively behavior similar to what we observe in Fig. 3; the region where the asymptotic expression represents $I_n(p_\perp, Q)$ accurately shrinks with n. Thus, the behavior of $W_n(p_\perp)$ is a consequence of the property of the integrals $I_n(p_\perp, Q)$ that the region where the linear in $|p_\perp|$ asymptotic takes over shrinks progressively with n.

This feature of $W_n(p_\perp)$ is quite important for understanding how the cusp in TEMD is produced. As Eq. (19) shows, the terms of the series (14) behave as linear functions of $|p_\perp|$ for small enough $p_\perp$. At first glance, that would suggest that the sum of the series (14), the TEMD $W(p_\perp)$, would exhibit the same behavior linear in $|p_\perp|$ near $p_\perp = 0$. That would imply the following cusp structure: TEMD would have discontinuous first and infinite second derivatives at $p_\perp = 0$. On the other hand, the cusps shown in Fig. 1 look more like functions of $p_\perp$ with an infinite first derivative. In other words, $W(p_\perp)$ grows visibly faster than $|p_\perp|$ near $p_\perp = 0$. This apparent contradiction is resolved when one realizes that $W(p_\perp)$ is a sum (14) of the terms $W_n(p_\perp)$. Each $W_n(p_\perp)$ behaves as a linear function of $|p_\perp|$ in some vicinity of $p_\perp = 0$, but as we saw above, the interval of $p_\perp$ in which linear dependence is a good approximation shrinks with n. If, as Fig. 3 suggests, outside the interval of applicability of the asymptotic law $W_n(p_\perp)$ grow slower with $p_\perp$ [we see this behavior for the integrals $I_n(p_\perp, Q)$ in Fig. 4], the sum of all $W_n(p_\perp)$ in (14) will exhibit precisely the behavior seen in Fig. 1: the growth is faster than linear for $p_\perp \to 0$. With $p_\perp \to 0$ the terms with higher n switch progressively from the relatively slow growth outside the asymptotic region to a faster growth linear in $|p_\perp|$ once $p_\perp$ is inside the region of the validity of the asymptotic law (19) for a particular n.

To see this quantitatively we introduce a function:

$$f(z) = \sum_{m=0}^{\infty} C_{2m} z^m \,, \tag{20}$$

where C_{2m} are the coefficients in Eq. (16) [the definition (20) takes into account that only the even-order coefficients C_n occur in Eq. (14)]. The function $f(z)$ in Eq. (20) is defined in terms of the set of coefficients C_n and encapsulates therefore information about the solution of the TDSE and, ultimately, information about the dynamics of the ionization process. For the sum of the series (14) we can then write [we omit the contributions of the regular parts $W_n^{\mathrm{reg}}(p_\perp)$ since they do not lead to the singular behavior]

$$\begin{aligned} I(p_\perp) &= \sum_{n=0,2,\ldots}^{\infty} C_n \int_0^Q dq \frac{q^{n+1}}{\left(p_\perp^2 + q^2\right)^{\frac{n+1}{2}}} \\ &= \int_0^Q \frac{q}{\sqrt{p_\perp^2 + q^2}} f\left(\frac{q^2}{p_\perp^2 + q^2}\right) dq. \end{aligned} \tag{21}$$

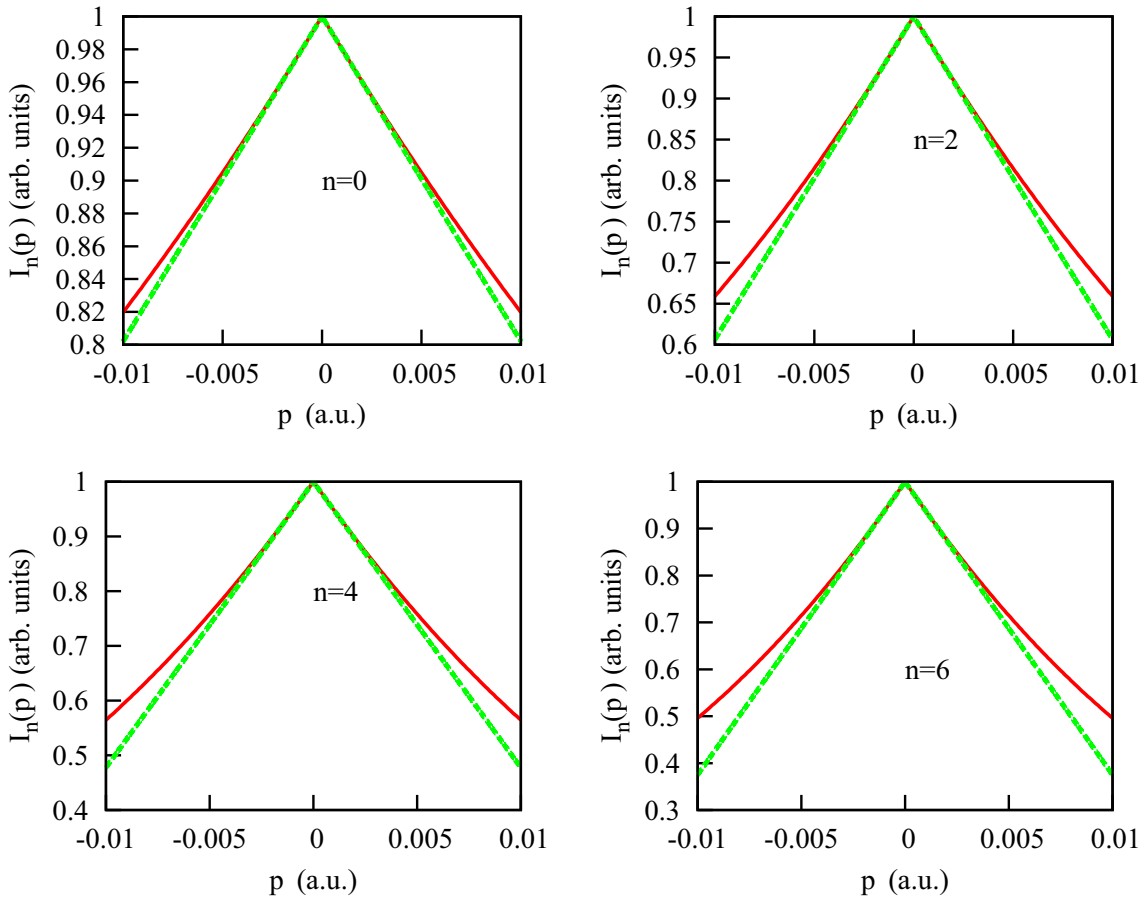

FIG. 4. (Color online) Solid red line: integrals $I_n(p_\perp, Q)$ as functions of lateral momentum $p_\perp$ for $Q = 0.05$. Dashed green line: linear fit, $I_n(p_\perp, Q) = A + B|p_\perp|$.

Substituting $y = \frac{p_\perp}{\sqrt{p_\perp^2+q^2}}$, we can rewrite Eq. (21) as

$$I(p_\perp) = p_\perp \int_{y(Q)}^{1} \frac{dy}{y^2} f(1-y^2), \tag{22}$$

where $y(Q) = \frac{p_\perp}{\sqrt{p_\perp^2+Q^2}}$.

Assuming that in this expression $f(z) = z^n$, which corresponds to all but one coefficients C_n in Eq. (16) having zero values, reproduces, of course, the asymptotic law (19) we obtained above for the individual terms $W_n(p_\perp)$ of the series (14). A more realistic assumption about $f(z)$ can be based on the observation we made above that the coefficients C_n are ultimately related to the partial-wave expansion of the solution of the TDSE equation. It is clear that to establish small-$p_\perp$ behavior of the sum of the series (14) we actually need to know only the large-n asymptotic behavior of C_n. Partial-wave expansions in the TDSE calculations converge, as a rule, rather slowly [18]. A plausible assumption about the large-n asymptotic behavior of the sequence of C_n, reflecting this slow convergence, would be a powerlike asymptotic behavior $C_n \propto n^{-\lambda}$ with some positive λ. By the well-known theorems of the complex analysis this implies the presence of at least one singular point of $f(z)$ on the circle of convergence $|z| = 1$. Let us assume, for example, that this singularity is a simple branch point at $z = 1$, so that $f(z) = \sqrt{1-z}$. We obtain then from Eq. (23)

$$I(p_\perp) = p_\perp \int_{y(Q)}^{1} \frac{dy}{y}, \tag{23}$$

which, as one can easily see, leads to the following formula for the asymptotic behavior of $I(p_\perp)$ for $p_\perp \to 0$:

$$I(p_\perp) = A + B|p_\perp| \ln|p_\perp| \quad p_\perp \to 0\,, \tag{24}$$

with some constants A and B. We see thus that while terms of the series (21) all have $|p_\perp|$ cusps at $p_\perp = 0$, the sum of the series (21) can exhibit more singular cusplike behavior at this point. For the terms of series (21) the first derivatives with respect to $p_\perp$ are discontinuous at $p_\perp = 0$, and the second derivative is infinite at $p_\perp = 0$. The cusp singularity of the sum of the series (21), with the choice of the function $f(z)$ we used above as an example, is more severe; the first derivative with respect to $p_\perp$ is infinite at $p_\perp = 0$.

Incidentally, the asymptotic law (24) reproduces fairly well the TEMD obtained in our TDSE calculations. As one can see from Fig. 5, the two-parameter formula $A + B|p_\perp| \ln|p_\perp|$ (A and B are considered fitting parameters) actually gives better results than the three-parameter fit based on the equation $W(p_\perp) = A + B|p_\perp|^\alpha$ (A, B, and α are fitting parameters). We cannot, of course, claim that $A + B|p_\perp| \ln|p_\perp|$ is the actual behavior of the TEMD $W(p_\perp)$ for small $p_\perp$. As we saw, to describe the cusp in the TEMD we rely on two ingredients.

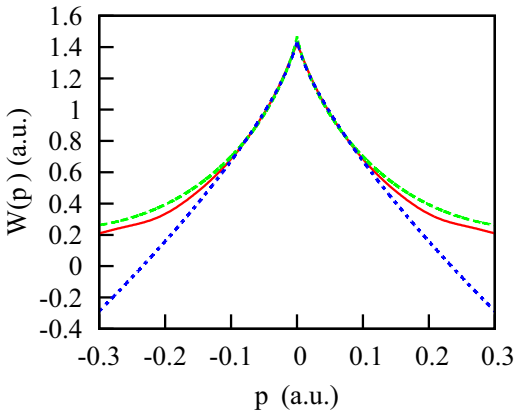

FIG. 5. (Color online) TEMD for a field intensity of 3.5×10^{14} W/cm^2 and pulse duration of four optical cycles. Solid red line: TDSE calculation. Long-dashed green line: fit based on the equation $W(p_\perp) = A + B|p_\perp| \ln|p_\perp|$ (fitting parameters A and B). Short-dashed blue line: fit based on the equation $W(p_\perp) = A + B|p_\perp|^\alpha$ (fitting parameters A, B, and α).

We need first to describe the small-$p_\perp$ behavior of the "partial" distributions $W_n(p_\perp)$ in (14). Equations (16) and (18) provide an answer to this problem. To find small-$p_\perp$ behavior of the sum of the series (14) we also need to know the weights with which different $I_n(p_\perp)$ in Eq. (16) contribute to the sum: the coefficients C_n in this equation. The logarithmic behavior in Eq. (24) obtains, in particular, assuming that $f(z)$ in Eq. (20), which encapsulates information about the coefficients C_n, has a simple branch point at $z = 1$, an assumption leading to apparently satisfactory results, which we, however, did not prove. We may therefore regard this formula as a plausible but only tentative expression.

III. CONCLUSION

We considered in detail the formation of the cusp in the TEMD for the process of strong-field ionization. As we saw, one can push the analytic approach to this problem quite far. Our starting point was the series (14) resulting from the expansion of the differential probability in the powers of $\cos\theta$, the angle between the polarization vector and the electron momentum. We were able to show that the terms $W_n(p_\perp)$ of this series behave as linear functions of $|p_\perp|$ for small $p_\perp$. This behavior is a consequence of the properties of the Coulomb continuous-spectrum wave functions and is present therefore for any system regardless of what the actual Hamiltonian is, as long as the wave function of the system after the end of the laser pulse is projected on the set of Coulomb wave functions. If this were the whole story, the TEMD would have the $|p_\perp|$ cusp at $p_\perp = 0$. For such a cusp the first derivative at $p_\perp = 0$ is discontinuous, and the second derivative is infinite.

There is, however, a second step we have to perform to obtain the TEMD. The functions $W_n(p_\perp)$ in (14) with the small-$p_\perp$ asymptotic behavior which we established in Eq. (19) constitute the building blocks from which TEMD can be built by summing up the expansion (14). It is at this stage that dynamic information, i.e., the information about particular details of the ionization process, becomes important. The partial lateral distributions $W_n(p_\perp)$ considered as functions of n enter the series (14) with different weights. Mathematically, this fact is reflected in Eq. (16), which represents $W_n(p_\perp)$ as a product of the integral $I_n(p_\perp)$ and a coefficient C_n which is a function of only n. The coefficients C_n depend, of course, on the dynamics of the system since they result ultimately from the projection of the TDSE wave function at the end of the laser pulse. The function we introduced in Eq. (20) conveniently encapsulates this information. As we saw, the summation procedure can make the character of the cusp for the sum of the series (14) different from the linear $|p_\perp|$ cusp that each of the terms of the series exhibits at $p_\perp = 0$. The reason for this is, roughly speaking, the fact that for the terms of the series (14) with higher n the region of lateral momenta for which linear in $|p_\perp|$ asymptotic law holds for $W_n(p_\perp)$ shrinks, or, in stricter mathematical language, the fact that the small-$p_\perp$ asymptotic behavior (19) for $W_n(p_\perp)$ is nonuniform in n.

To summarize, we demonstrated that the cusp in the TEMD arises as a consequence of two factors: The singularity of the Coulomb wave function produces a simple cusp of the $A + Bp_\perp$ type. The view expressed in [13] that the cusp is due to the singularity of the Coulomb scattering state is therefore basically correct; the Coulomb wave function is responsible for the presence of the cusp. This fact has nothing whatsoever to do with the dynamics of the photoionization process. The character of the cusp we observe in the TEMD, however, may differ from the $A + Bp_\perp$ type created by the Coulomb wave function. The origin of this difference lies in the dynamics; it is ultimately due to the properties of the coefficients of the expansions (13) and (14), which depend on the wave function at the end of the laser pulse.

ACKNOWLEDGMENT

This work was supported by the Institute for Basic Science under Grant No. IBS-R012-D1.

[1] L. V. Keldysh, Sov. Phys. JETP **20**, 1307 (1965).
[2] F. H. M. Faisal, J. Phys. B **6**, L89 (1973).
[3] H. R. Reiss, Phys. Rev. A **22**, 1786 (1980).
[4] A. M. Perelomov, V. S. Popov, and M. V. Terentiev, Sov. Phys. JETP **23**, 924 (1966).
[5] M. V. Ammosov, N. B. Delone, and V. P. Krainov, Sov. Phys. JETP **64**, 1191 (1986).
[6] V. S. Popov, Phys. Usp. **47**, 855 (2004).
[7] S. V. Popruzhenko, J. Phys. B **47**, 204001 (2014).
[8] N. I. Shvetsov-Shilovski, D. Dimitrovski, and L. B. Madsen, Phys. Rev. A **85**, 023428 (2012).
[9] R. Boge, C. Cirelli, A. S. Landsman, S. Heuser, A. Ludwig, J. Maurer, M. Weger, L. Gallmann, and U. Keller, Phys. Rev. Lett. **111**, 103003 (2013).
[10] A. N. Pfeiffer, C. Cirelli, A. S. Landsman, M. Smolarski, D. Dimitrovski, L. B. Madsen, and U. Keller, Phys. Rev. Lett. **109**, 083002 (2012).
[11] S. V. Popruzhenko, J. Exp. Theor. Phys. **118**, 580 (2014).

[12] L. Arissian, C. Smeenk, F. Turner, C. Trallero, A. V. Sokolov, D. M. Villeneuve, A. Staudte, and P. B. Corkum, Phys. Rev. Lett. **105**, 133002 (2010).
[13] A. Rudenko, K. Zrost, T. Ergler, A. B. Voitkiv, B. Najjari, V. L. B. de Jesus, B. Feuerstein, C. D. Schröter, R. Moshammer, and J. Ullrich, J. Phys. B **38**, L191 (2005).
[14] I. A. Ivanov, Phys. Rev. A **90**, 013418 (2014).
[15] I. A. Ivanov, A. S. Kheifets, J. Calvert, S. Goodall, X. Wang, H. Xu, A. Palmer, D. Kielpinski, I. Litvinyuk, and R. T. Sang, arXiv:1503.04891.
[16] I. A. Ivanov, Phys. Rev. A **83**, 023421 (2011).
[17] I. A. Ivanov and A. S. Kheifets, Phys. Rev. A **87**, 033407 (2013).
[18] M. Nurhuda and F. H. M. Faisal, Phys. Rev. A **60**, 3125 (1999).
[19] L. D. Landau and E. M. Lifshitz, *Quantum Mechanics* (Pergamon Press, New York, 1977).
[20] M. Abramowitz and I. E. Stegun, *Handbook of Mathematical Functions* (National Bureau of Standards, Washington, D.C., 1967).